Seismic Vulnerability Analysis of Irregular Multi-Span Concrete Bridges with Different Corrosion Damage Scenarios

Ebrahim Afsar Dizaj[a*], **Mohammad R. Salami**[b], **Mohammad M. Kashani**[c]

[a]Assistant Professor, Department of Civil Engineering, Azarbaijan Shahid Madani University, Tabriz, Iran. (corresponding author), Email: ebrahim.afsardizaj@azaruniv.ac.ir

[b]Senior Lecturer in Civil Engineering, School of Engineering and the Built Environment, Birmingham City University, B5 5JU, United Kingdom, Email: mohammad.salami@bcu.ac.uk

[c]Associate Professor, Faculty of Engineering and Physical Sciences, University of Southampton, Southampton, SO17 1BJ, United Kingdom, Email: mehdi.kashani@soton.ac.uk

Abstract

This paper investigates the seismic performance and vulnerability of multi-span Reinforced Concrete (RC) bridges with unequal height piers exposed to varied corrosion damage scenarios. An advanced three-dimensional nonlinear finite element modelling technique is developed and verified with available experimental results of a reference shake table test on a large-scale RC bridge. In addition to the pristine state of the reference bridge, various hypothetical corrosion scenarios, including the symmetrical and asymmetrical corrosion of piers, are considered. Several nonlinear analyses, including the pushover and Incremental Dynamic Analysis (IDA) approach, are performed to evaluate the seismic behaviour and vulnerability of hypothetical RC bridge specimens. The influence of symmetrical and asymmetrical corrosion of piers on nonlinear dynamic behaviour and failure mechanism (both in the global and local scales) of studied bridges are then discussed. Finally, the IDA results are used to develop time-dependent fragility curves. The analyses show that seismic vulnerability of a deteriorated irregular multi-span RC bridge

crucially depends on the corrosion scenario of its piers, where the unbalanced distribution of seismic ductility demand might be regulated/intensified by different corrosion scenarios. Moreover, some corrosion scenarios resulted in near-synchronised failure of unequal height piers.

Keywords: Concrete bridge; Fragility curve; Incremental dynamic analysis; Corrosion; Irregularity; Synchronised failure; Seismic vulnerability

1. Introduction

Bridges, major transport infrastructure artefacts, pervade everyone differently; they are part of daily life for most and are an essential and critical part of the global economy and society. The integrity and performance of existing ageing transport infrastructures in the extreme environment should be preserved in any condition as they are critical strategic communication pathways, which will result in disruption of the whole transportation network if they lose their functionality [1-3].

In recent years, corrosion-induced deterioration of concrete bridges has been turned into the main challenge of bridge owners and stakeholders [4-5]. Severe corrosion and insufficient reinforcement details have resulted in several catastrophic failures worldwide (e.g., the collapse of the Morandi bridge in Italy [6]). A report published by Department for Transport and Highways England shows that corrosion damage to RC bridges costs about £1 billion/year in England and Wales, representing about 10% of the total UK bridge inventory [3-4, 7]. In the US, the estimated direct cost to repair ageing infrastructure is over $200 billion in total [4, 8].

Additionally, the experience of past catastrophic earthquakes, such as the Irpinia earthquake in 1980 and the L'Aquila earthquake sequence in 2009 [9], has been raised the concern of the engineering community about the joint consequences of seismic hazard and time-variant deterioration of corrosion-damaged RC bridges. Numerous studies have been carried out in the literature concerning the seismic performance of corrosion-damaged RC bridges [10-18]. The outcome of these studies shows that the corrosion-induced damage remarkably increases the vulnerability of RC bridges. Nevertheless, due to the significant scarcity of experimental data and advanced nonlinear material models in the literature, other damage parameters, such as the negative influence of corrosion on inelastic buckling and low-cycle fatigue degradation of reinforcement, have been ignored in these studies. Disregarding these aspects in numerical modelling approaches can significantly overestimate the energy dissipation capacity of corroded elements [19].

Several concrete bridges are located in rugged topography or irregular topographical surfaces that practical considerations impose on constructing them with irregular substructure, i.e., unequal height piers [20]. The irregularity associated with the substructure of such bridges results in unbalanced seismic demand in piers of varied stiffnesses, where the stiffer piers attract greater seismic inertia forces and ductility demands. A significant deal of research has been dedicated to investigating the seismic behaviour of irregular multi-span RC bridges [21-30]. The state-of-the-art studies on the seismic performance and irregularity criteria of concrete bridges are comprehensively reviewed by Akbari and Maalek [23]. A number of these studies aim to propose a practical methodology to mitigate the unbalanced seismic response of these bridges due to the substructure irregularity [20, 31]. However, these studies have not considered the combined effect of corrosion and stiffness irregularity.

Previous research on seismic vulnerability assessment of corrosion-damaged RC bridges is typically carried out by assuming a symmetrical corrosion scenario, where for the sake of simplicity, the average time-varying corrosion level of piers is supposed to be the same during the service life [5, 12, 15, 32-33]. However, depending on several environmental and exposure conditions, different components of a multi-span RC bridge might experience varying degrees of corrosion at the same time in its service life. Bridges are typically constructed over highways, railways, rivers, and/or valleys, leading to different corrosion patterns in piers. For instance, if part of a multi-span bridge is constructed over a highway and the other part over a valley, the piers adjacent to the highway will experience more severe corrosion due to the use of de-icing salt on highways in winter.

Moreover, the seismic response of bridges with substructure irregularity can be crucially affected if they are located in corrosive environments. The complexity in seismic response of such bridges can be further increased if piers of varying heights are exposed to asymmetrical chloride-induced corrosion levels. This asymmetrical corrosion of piers can exacerbate the unbalanced seismic demand, leading to varied transverse seismic responses of such bridges. Additionally, it can affect the damage mechanisms, change the pattern of demand absorption and alter the failure sequence of different bents. Nonetheless, such aspects have not been highlighted in any previous studies. This paper aims to address the shortcoming in the literature by extensively investigating the seismic performance of irregular asymmetrically corroded bridges, as explained in detail in the following section.

1.1 Research Contribution and Novelty

The above discussion shows a significant scarcity in the literature on seismic performance evaluation and vulnerability analysis of irregular multi-span RC bridges subject to different corrosion-induced damage scenarios. Most of the previous studies on seismic fragility analysis of corroded bridges have used simplified corrosion models that were not able to capture multiple failure modes of RC structures [5, 12, 16]. Furthermore, there has been no study on nonlinear dynamic behaviour and seismic fragility analysis of ageing irregular multi-span bridges with corrosion damage. Therefore, for the first time, this study aims to address this shortcoming in the literature by investigating the nonlinear dynamic behaviour and seismic vulnerability analysis of multi-span RC bridges with substructure irregularity subject to different symmetrical and asymmetrical corrosion scenarios. To this end, an advanced three-dimensional finite element (FE) modelling technique, which is able to predict multiple failure modes of RC components, is employed. The FE model includes corrosion damage models that account for the impact of corrosion on mechanical properties, inelastic buckling, and low-cycle fatigue degradation of longitudinal reinforcement, as well as mechanical properties of confining reinforcement resulting in premature core concrete crushing. The proposed detailed FE model at the component level is implemented in a 3D model of a multi-span irregular bridge with different corrosion damage scenarios. The developed model is employed to estimate the time-dependent seismic damage limit states of a case-study two-span irregular RC bridge with various corrosion scenarios, which are subsequently used in seismic performance and fragility analyses.

The developed FE model is validated against experimental results of a large-scale shake table test on a benchmark multi-span RC bridge with unequal pier heights, available in [34]. Subsequently, employing nonlinear pushover and incremental dynamic analyses (IDAs), the influence of different corrosion scenarios (including symmetrical and asymmetrical corrosion scenarios) on seismic behaviour and fragility of RC bridges with irregular substructure is investigated. The seismic behaviour and failure analysis of the hypothetical bridges with various corrosion scenarios are presented in both the global and material scales to investigate the complex seismic behaviour of irregular RC bridges with corroded piers. The obtained results indicate that uneven (asymmetrical) corrosion of unequal height piers can affect the unbalanced distribution of seismic ductility demands and cause the near-simultaneous failure of piers. Although these results are based on a case-study bridge, they provide an insight into the significance of corrosion impact on nonlinear seismic behaviour of such bridges. Furthermore, the proposed 3D modelling strategy that is developed in this paper for the case-study bridge provides a guidance to other researchers and bridge engineers to be used in future studies.

2. Finite Element Model and Verification

2.1 Structural Details of Reference RC Bridge

Johnson et al. [34] conducted multiple large-scale shake table tests on a two-span post-tensioned RC bridge using the shake table facility available at the University of Nevada, Reno. The primary objective of the project, which was a component of a collaborative multi-university project, was to study the influence of in-plane rotation on the seismic response of an asymmetric RC bridge under transverse excitations. Therefore, a quarter-scale two-span RC bridge specimen resting on three bents of varying heights was cast-in-place in the laboratory. The bridge was then subjected to two successive lateral excitation sets, including 11 low-amplitude tests and the subsequent eight high-amplitude tests with increasing intensities. The first set was intended to induce pre-yield slight damages in the columns, while the second (i.e., high-amplitude) runs were performed in increased intensity sequences to cover the performance of the bridge from the first yielding of reinforcement up to the failure of the first bent.

Fig. 1 shows the configuration and geometry of the two-span RC bridge system tested by Johnson et al. [34]. This bridge represents a middle frame of multiple-frame RC bridges with varying pier heights, where the tallest of columns are located in the middle (bent 2), the shortest of columns in bent 3, and the medium-height columns in bent 1. The clear span lengths are approximately 8 m, and the total height of the bridge is 3.25 m, where the clear height of columns in bent 1, bent 2 and bent 3 are 1.83 m, 2.44 m, and 1.53 m, respectively. This asymmetric pattern of columns with varied stiffnesses causes an altitudinal irregularity of the bridge in the transverse vibration. As Fig. 1 shows, a series of superimposed masses in the shape of concrete blocks and lead pallets are placed on the bridge deck. These superimposed masses and the self-weight of concrete provide an approximately axial load ratio of 0.082 on each pier. Other detailed information on the bridge geometry and configuration can be obtained from a 3D system overview presented in Fig. 1.

In Fig. 2 the geometry and structural details of each bent and column are shown. As Fig. 2 shows, all the bridge piers have the same circular cross-section with a diameter of 305 mm, 16 number of 9.5 mm (#3 bars) steel rebars as the vertical reinforcement, and 4.9 mm spiral reinforcement pitched at 32 mm on the centre. The clear spacing of the columns of each bent in the transverse direction is 1.6 m. In Table 1, the details of material properties and geometrical specifications of the bridge columns are summarised. Further information on the details and experimental setup of the bridge can be found in [34].

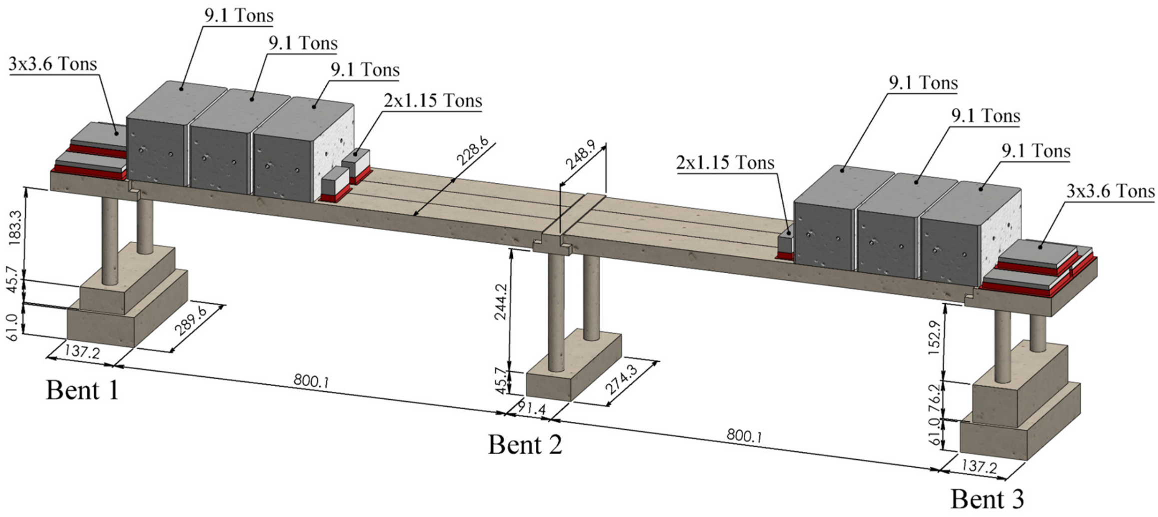

Fig. 1. 3D view of the reference irregular RC bridge (dimensions in cm)

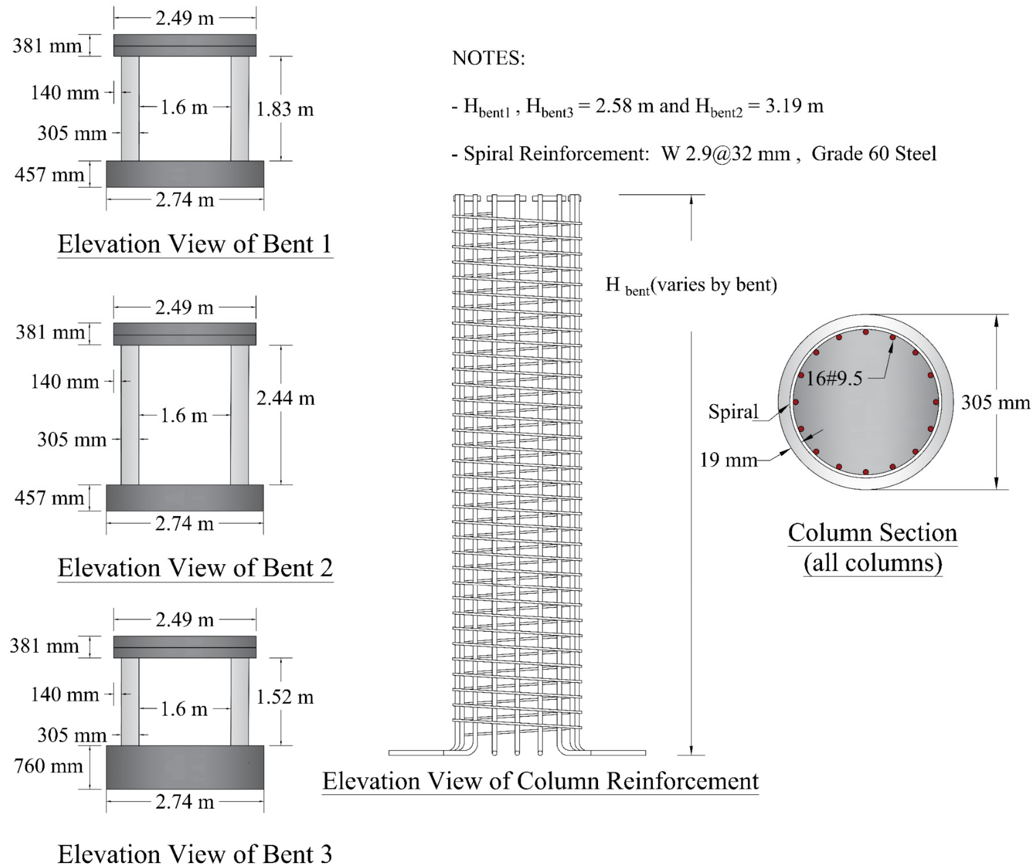

Fig. 2. Details and geometry of the substructure components

Table 1. Material and geometrical properties of the columns in different bents

Bent No.	L (m)	L/D	ρ_l (%)	ρ_s (%)	$N_u/(f_c A_g)$	f_c (MPa)	f_y (MPa)	f_u (MPa)	f_{yh} (MPa)
Bent 1	1.83	3	1.56	0.9	0.082	40.7	459	669	462
Bent 2	2.44	4	1.56	0.9	0.082	40.7	459	669	462
Bent 3	1.52	2.5	1.56	0.9	0.082	40.7	459	669	462

Column height (L), shear span to depth ratio (L/D), the ratio of the longitudinal bars (ρ_l), the volumetric ratio of spiral reinforcement (ρ_s), axial force ratio ($N_u/f_c A_g$), compressive strength of concrete (f_c), yield strength of longitudinal reinforcement (f_y), the ultimate tensile strength of longitudinal reinforcement (f_u), and the yield strength of spiral reinforcement (f_{yh}).

2.2 Details of Developed 3D FE Model

In this study, the specifications of the irregular RC bridge tested by Johnson et al. [34] are considered as a reference to investigate the seismic vulnerability of RC bridges with varied pier heights subject to different corrosion scenarios. The first step is to develop a reliable numerical model capable of accurately simulating the nonlinear response of the system and the possible secondary effects such as buckling, fatigue, spalling, etc., due to the corrosion of rebars.

Fig. 3(a) shows the three-dimensional nonlinear finite element model of the bridge developed in OpenSees platform [35]. In this figure, the structural nodes and the overall configuration of the model are shown. As Fig. 3(a) shows, some nodes are defined in an elevated coordinate with respect to the bridge deck (e.g., node 481). These nodes are defined to apply the superimposed masses in their exact mass centres and are connected to elastic beam-column elements of the bridge deck by rigid links. The reason for using elastic beam-column elements for the deck beams (and beam caps) is that these components are designed to remain in the elastic range during all the shake table tests [34].

In bridge systems, piers are the most critical components that determine the nonlinear seismic behaviour of the whole system. Therefore, special attention should be paid to accurate nonlinear structural behaviour modelling of these elements. To this end, the nonlinear fibre beam-column element (NFBCE), available in the Opensees [35], is used to simulate the nonlinear response of RC bridge piers. The corrosion damage models proposed by Kashani et al. [36] are implemented in the NFBCE, which can simulate the effects of corrosion on premature inelastic buckling, low-cycle fatigue degradation, premature spalling of concrete cover, premature fracture of reinforcing bars in tension, and premature core concrete crushing due to corrosion of confining reinforcement. The accuracy and effectiveness of this model have been validated against an extensive number of experimental results [36]. For instance, Fig. 3(b) shows a two-dimensional view of the proposed FE model of bent 1 to give extra details. In this figure, the nodal labels, as well as different elements of columns, are shown. As Fig. 3(b) shows, two zero-length section elements (available in OpenSees) are used to consider the bond-slip effects in the bottom and top connection regions for each column. The force-based elements with three integration points (Element 1 and Element 3) are used in the bottom and top critical regions to address the strain localisation problems due to the softening behaviour of reinforcement in compression.

A force-based element with five integration points is used for the middle element (Element 2). The rigid links connecting nodes 6 and 13 to nodes 7 and 14, respectively (Fig. 3(b)), are considered to model the rigid region in column-beam cap connection. The nonlinear stress-strain behaviour of concrete is simulated using the *Concrete04* uniaxial material model available in OpenSees. The confinement effects on the ductility and strength of confined core concrete are taken into account using the model proposed by Mander et al. [37]. The nonlinear behaviour of reinforcement is modelled using the phenomenological hysteretic buckling model proposed by Kashani et al. [38].

All the column to foundation connections are considered to be fully fixed. The P-delta effects are considered in the model through the P-delta transformation object available in OpenSees. Further details on the nonlinear finite element beam-column element of bridge piers are available in the systematic modelling guidelines proposed by Afsar Dizaj and Kashani [11].

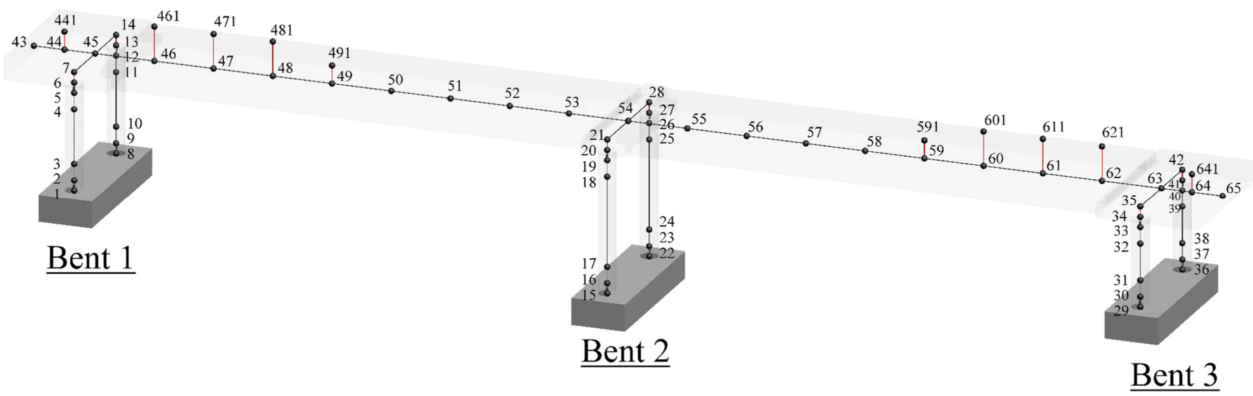

(a)

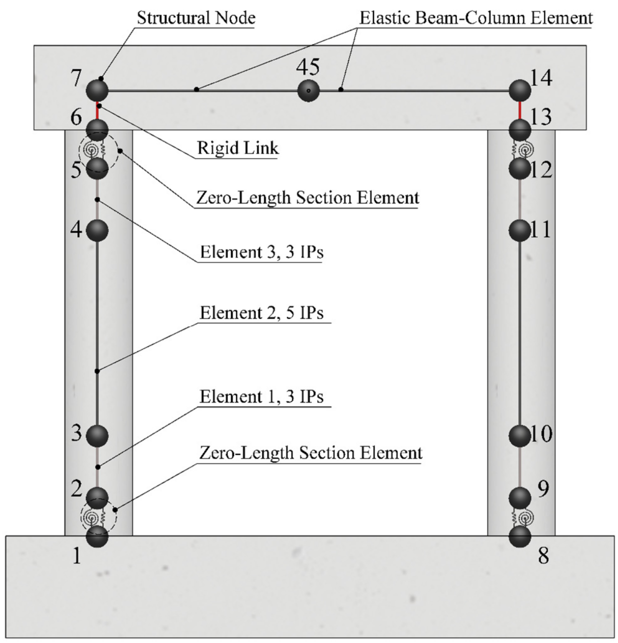

(b)

Fig. 3. Nonlinear finite element model of the bridge: (a) 3D view of the bridge model, and (b) 2D view of the FE model of bent 1

2.3 Validation of the FE Model

The high-amplitude shake table test outputs are used herein to validate the developed three-dimensional nonlinear FE model of the reference bridge. To this end, the multiple support excitation loading pattern (available in OpenSees) is used to apply the displacement time histories achieved on the three shake tables as inputs for the numerical model. The reason for using displacement time histories instead of acceleration time histories of the tables is that the latter were incoherent due to the interaction between the bridge system and the three shake tables. Further details can be found in [34].

Fig. 4 shows an exemplar result of numerical verification, where the predicted acceleration responses of different bents under high-amplitude test 16 are compared with the shake table test results. As seen in this figure, the simulated response shows a desirable match to the experimental results. To further investigate the validity of the model, in Fig. 5, the simulated hysteretic acceleration-displacement response of each bent is compared with the corresponding output of the experiment during test 12. The results presented in this figure show that the simulated responses are nearly identical to the experimental outputs.

The above discussion confirms the validity and accuracy of the developed numerical model in predicting the nonlinear seismic response of the reference bridge system under transverse earthquake excitation loading. Therefore, this model is used in the next section of the paper to study the vulnerability of irregular multi-span RC bridges with different corrosion scenarios subject to transverse seismic loading.

It is noteworthy that, at the component level, the proposed finite element modelling technique has been validated against experimental results of several uncorroded and corroded RC bridge columns. The details of these validations are available in [11, 36].

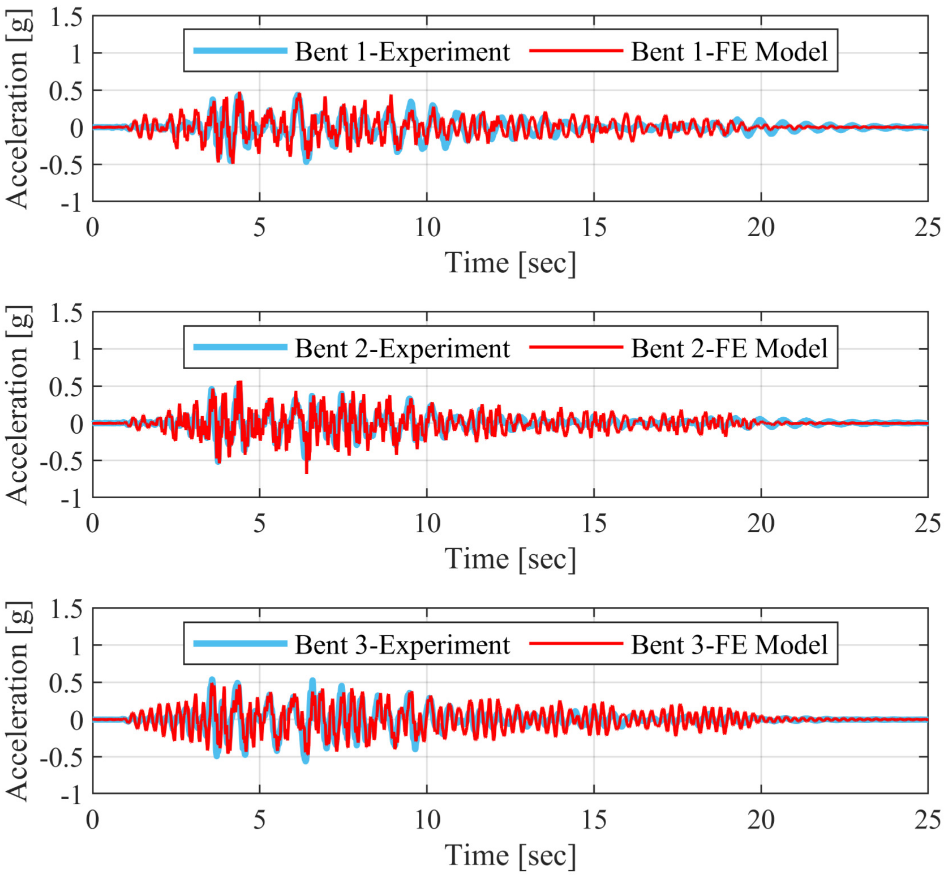

Fig. 4. Numerical validation results for different bents of the reference bridge under high-amplitude test 16

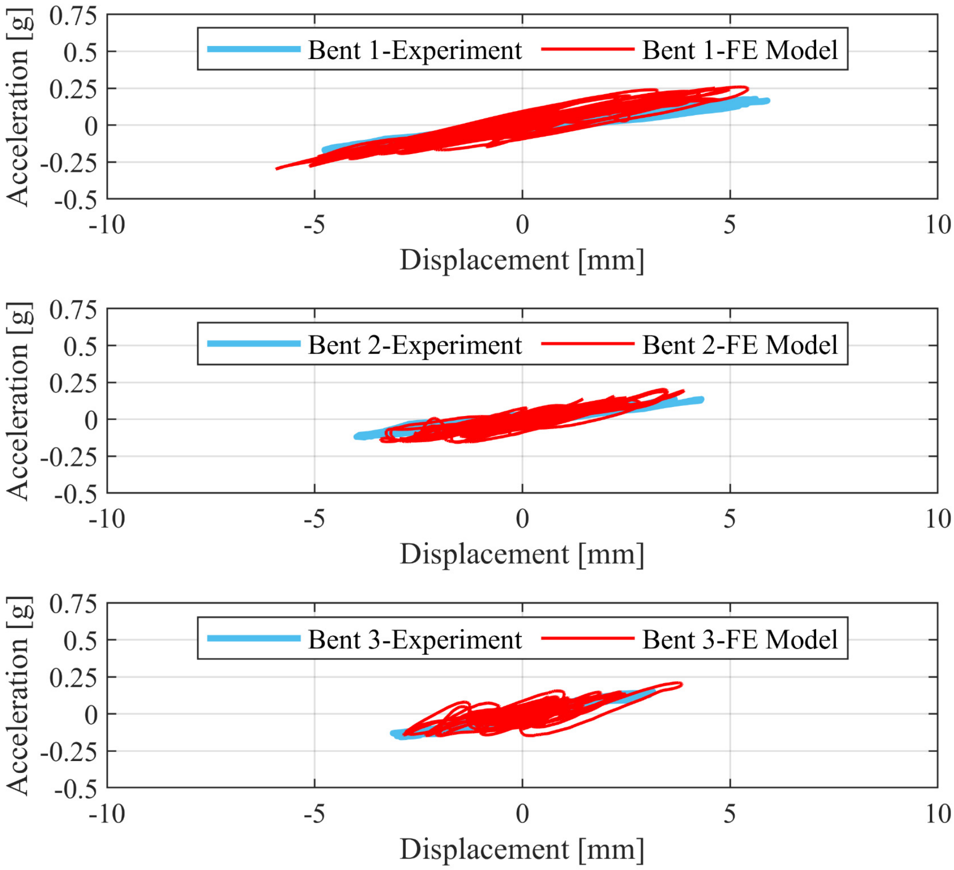

Fig. 5. Validating the hysteretic response of different bents against the experimental results of the reference bridge under high-amplitude test 12

2.4 Modelling Corrosion Effects

Several experimental and computational studies have been carried out to quantify the degradation in material (steel and concrete) properties due to reinforcement corrosion [39-42]. Among the numerous available models, the following equations are widely used in the literature to apply the adverse corrosion effects on material strength and ductility:

$$\eta_c = [1-\beta\psi]\eta_p \quad (1)$$

$$\sigma_c = \frac{\sigma_p}{1+\lambda \frac{\varepsilon_{ave}}{\varepsilon_{c0}}} \tag{2}$$

$$\varepsilon_{uc,c} = 0.004 + 1.4\left[\frac{\rho_{s,c}\sigma_{ys,c}\,\varepsilon_{us,c}}{\sigma_{cp,c}}\right] \tag{3}$$

$$\rho_{s,c} = \left[1-0.0001\psi_s\right]\rho_s \tag{4}.$$

In Eq. (1), η_c denotes a generic mechanical property of corroded steel reinforcing bars, and η_p is the related property of pristine rebar (with no corrosion); β is a pitting corrosion coefficient, and ψ is the mass loss ratio of corroded bars. The value of β varies for different mechanical properties of steel rebars in tension and compression [41-42, 38].

Eq. (2) presents the relationship proposed in [40] for reducing the compressive strength of unconfined cover concrete due to excessive corrosion-induced cracking. In this equation, σ_c and σ_p represent compressive strength of corrosion-damaged and pristine cover concrete, respectively; λ is a constant factor equal to 0.1; ε_{c0} is the strain corresponding to σ_p, and ε_{ave} is the average tensile strain in corrosion-induced cracked cover concrete.

Eq. (3) presents the equation used in this study to modify the ultimate compressive strain of confined concrete. In Eq. (3), $\varepsilon_{uc,c}$ is the modified ultimate compressive strain of corrosion-damaged confined concrete; $\sigma_{cp,c}$ is the compressive strength of confined concrete with corrosion-damaged spiral reinforcement, and $\rho_{s,c}$ is the volumetric ratio of corroded spiral bars according to Eq. (4). In Eq. (4), ψ_s is the mass loss ratio of spirals.

In Eqs. (1-4), the mass loss ratio of steel rebars can be calculated using Eq. (5) [43]:

$$\psi = \left(\frac{d_b d_c - 1.05(1 - W/C)^{-1.64} t^{0.71}}{d_b d_c} \right)^2 \tag{5}$$

where d_b (in mm) is the bar diameter (either longitudinal rebar or spirals); d_c (in mm) is the cover to the surface of rebars; W/C is the water to cement ratio, and t (in years) is the time from corrosion initiation. In this study, the W/C is considered to be 0.4.

As an example, in Figs. (6-8), the nonlinear stress-strain backbone curves of steel rebars, concrete cover and core concrete are shown for pristine (ψ=0) and 19% corrosion (ψ=19%) statuses. Further details on the constitutive relationship of material models employed in this study and step-by-step guidelines to consider the adverse influence of corrosion damage on steel and concrete material models are presented in [11].

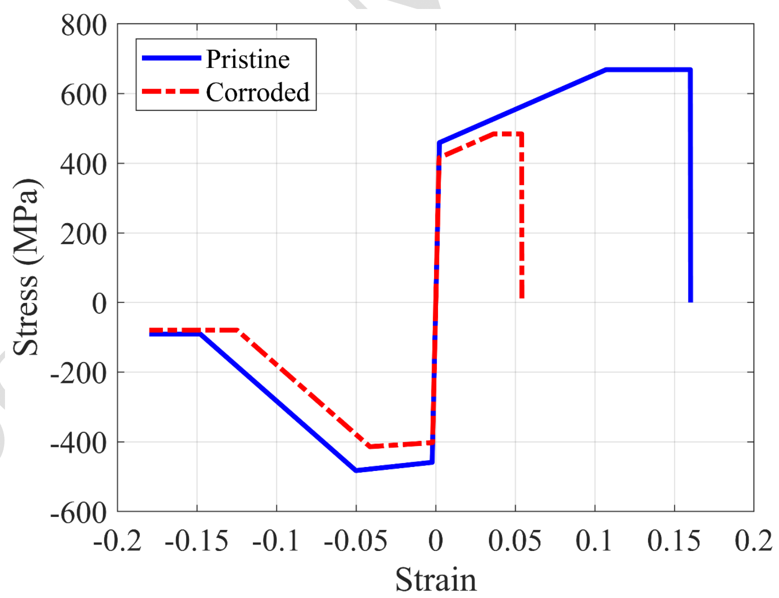

Fig. 6. Stress-strain backbone curve of pristine and extremely corroded reinforcement

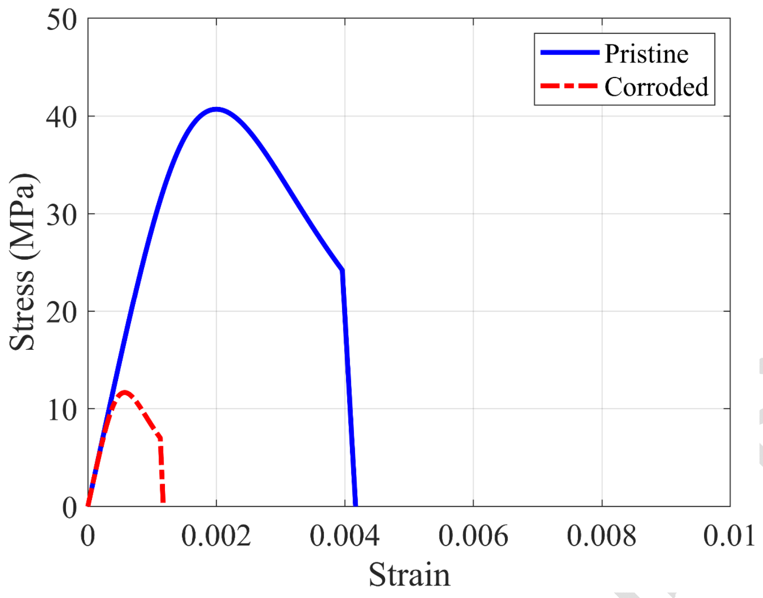

Fig. 7. Compressive stress-strain behaviour of pristine and extremely corroded concrete cover

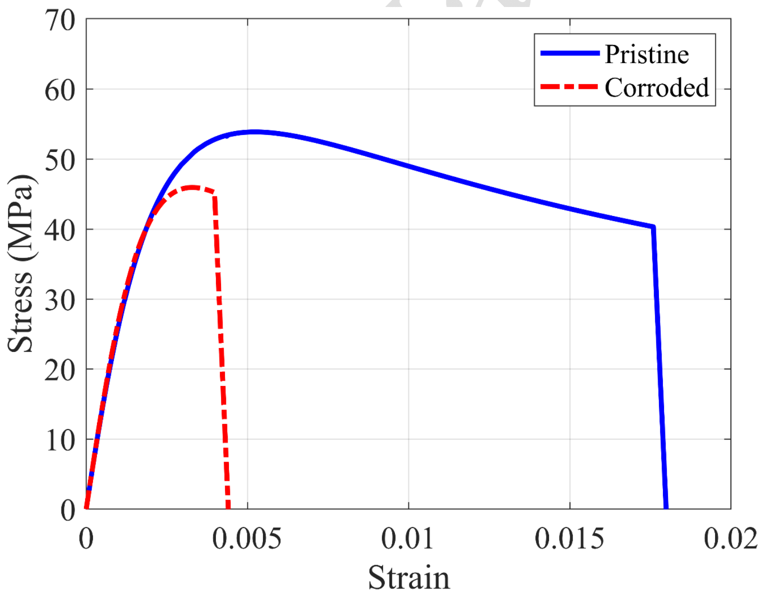

Fig. 8. Compressive stress-strain behaviour of pristine and extremely corroded core concrete

2.5 Symmetrical and Asymmetrical Corrosion Scenarios

In order to investigate the influence of corrosion on the seismic vulnerability of the case-study irregular RC bridge, different corrosion scenarios are considered. Table 2 lists the proposed corrosion scenarios. Scenario 1 is the reference bridge specimen tested by Johnson et al. [34] where all the piers are considered to be uncorroded. In scenario 2, all the piers are considered to be slightly symmetrically corroded. To this end, it is assumed that the bridge is in the status of 5 years after corrosion initiation (t=5 years), where using Eq. (5), the mass loss ratio of longitudinal and spiral reinforcement is calculated as 5.5% and 15.8%, respectively that can be considered as a slight corrosion level according to previous studies of the authors of the current paper [44]. In scenario 3, the bridge piers are considered to be in a long-time exposure to a corrosive environment, where 30 years have passed since the onset of reinforcement corrosion (t=30 years). In this condition, the mass loss ratio of longitudinal and spiral reinforcement will be approximately 18.9% and 50%, respectively. Therefore, in scenario 3 all piers are extremely symmetrically corroded.

Other than the symmetrical corrosion conditions considered in scenarios 2 and 3, two asymmetrical corrosion statuses are considered in which the corrosion degrees of different piers are assumed to be dissimilar at a given time. To this purpose, in scenario 4 the middle piers (piers of bent 2) are assumed to be severely corroded while the others are slightly corroded. Moreover, in Scenario 5, the shorter piers (piers in bent 3) are severely corroded, while piers of bent 1 and bent 2 are slightly corroded.

Table 2. The considered corrosion scenarios for the studied RC bridge

Scenario No.	**Corrosion status**			**Schematic view of the bridge**
	Bent 1	**Bent 2**	**Bent 3**	

1	pristine	pristine	pristine	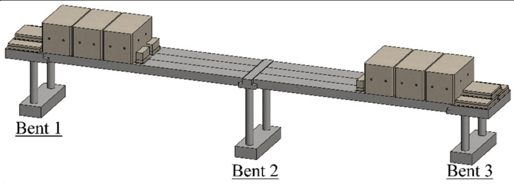
2	slightly corroded	slightly corroded	slightly corroded	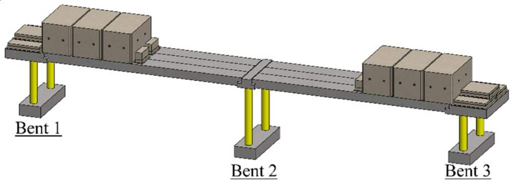
3	extremely corroded	extremely corroded	extremely corroded	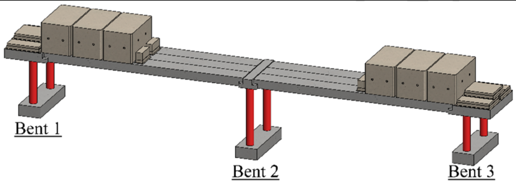
4	slightly corroded	extremely corroded	slightly corroded	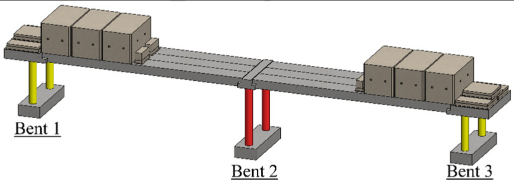
5	slightly corroded	slightly corroded	extremely corroded	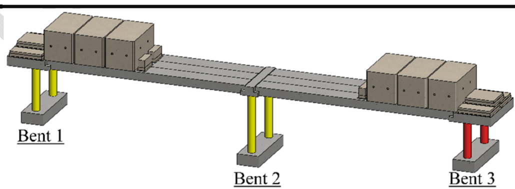

3. Pushover Analysis and Time-Dependent Seismic Damage Limit States

In seismic vulnerability assessment of structures, an explicit definition of different seismic damage limit states should be employed. Various references have described damage states for different components of bridges [5, 45-46]. However, the conventional definition of damage thresholds does not account for the time-dependent degradation of the material. One interesting approach emerging in recent years is defining limit states at the local level and translating them to the global level [47-48]. This latter approach allows updating the damage states in the structures/infrastructures lifetime at any given time. In this study, the second approach is employed. To this end, the capacity of each bent with different hypothetical corrosion statuses (i.e. pristine, slightly corroded, and severely corroded) is analysed by employing nonlinear pushover analysis.

During each analysis, the stress-strain response of core concrete and cover concrete at their extreme compression fibre, and the material response of the outmost tensile bar are recorded. From the analysis results, the drift ratio associated with the onset of reinforcement yielding (Δ_y), cover spalling (Δ_s), and core concrete crushing (Δ_c) are extracted as tabulated in Table 3. It is noteworthy that the drift ratio is defined here as the tip displacement of a bridge column divided by its height. Further details on the extraction of damage limit state capacities can be found in the systematic modelling guidelines provided in [11].

Fig. 9 shows the capacity curves of each bent subject to different corrosion levels. The drift ratios associated with rebar yielding, cover concrete spalling, and core concrete crushing are shown on each curve. It should be noted that the fracture of longitudinal reinforcement did not occur in any of the selected bridge layouts with varied corrosion levels. Moreover, because the onset of core concrete crushing occurred prior to a significant drop in capacity curves, it is considered as the onset of the collapse. As Fig. 9 shows, the capacity and ductility of each bent significantly deteriorate as the corrosion level increases. Notably, the extremely corroded bents experience a sudden drop in their post-peak response, showing a remarked decrease in their ductility.

The results obtained in this section are used in Section 4 and 5 to analyse the failure sequence and seismic fragility of bents in each hypothetical corrosion scenario.

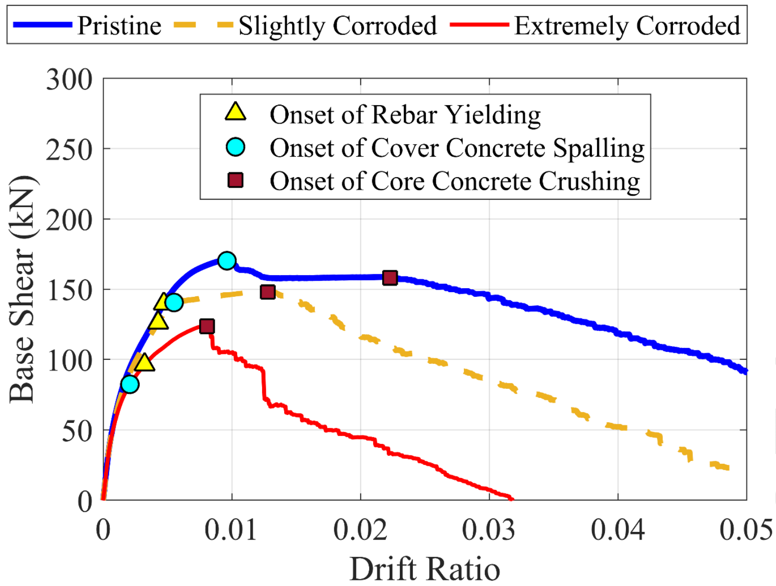
Pristine
Slightly Corroded
Extremely Corroded
Onset of Rebar Yielding
Onset of Cover Concrete Spalling
Onset of Core Concrete Crushing
Base Shear (kN)
Drift Ratio
300
250
200
150
100
50
0
0.01
0.02
0.03
0.04
0.05

(a)

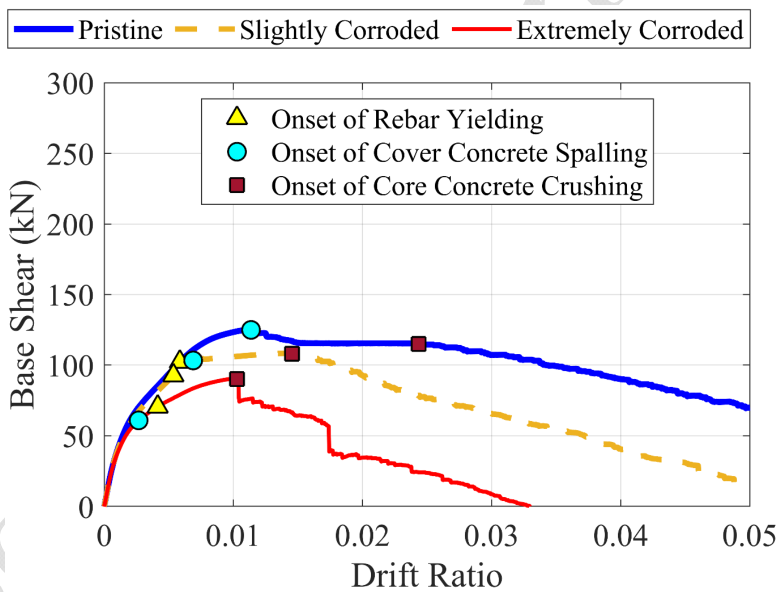
Pristine
Slightly Corroded
Extremely Corroded
Onset of Rebar Yielding
Onset of Cover Concrete Spalling
Onset of Core Concrete Crushing
Base Shear (kN)
Drift Ratio
300
250
200
150
100
50
0
0.01
0.02
0.03
0.04
0.05

(b)

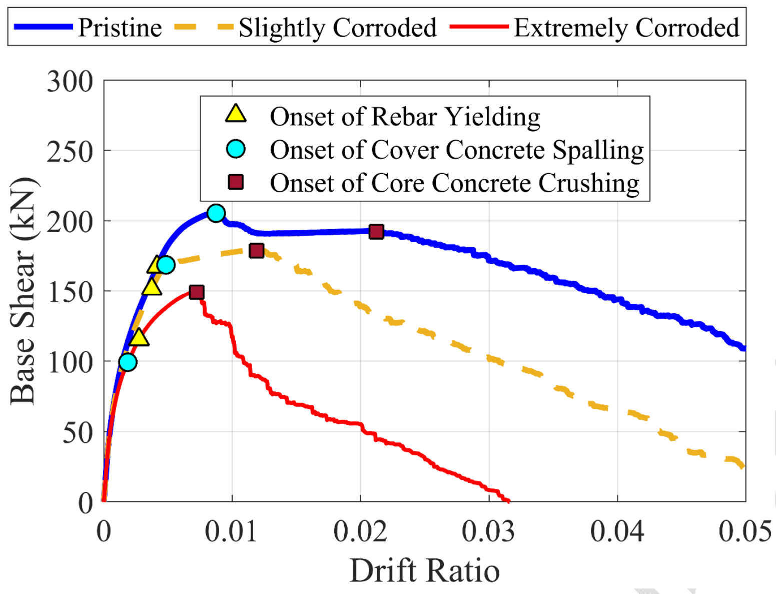

(c)

Fig. 9. Capacity curves of each bent for various corrosion levels of piers: (a) bent 1, (b) bent 2, and (c) bent 3.

Table 3. Drift ratios associated with the damage limit states

Bent No.	Corrosion Status	Δ_y	Δ_s	Δ_c
Bent 1	Pristine	0.0047	0.0096	0.0223
	Slightly corroded	0.0043	0.005	0.0128
	Severely corroded	0.0032	0.0021	0.0081
Bent 2	Pristine	0.0059	0.0114	0.0243
	Slightly corroded	0.0054	0.0069	0.0145
	Severely corroded	0.0041	0.0027	0.0103
Bent 3	Pristine	0.0041	0.0087	0.0212
	Slightly corroded	0.0037	0.0048	0.0119
	Severely corroded	0.0027	0.0019	0.0072

4. Incremental Dynamic Analysis

This section investigates the influence of different corrosion scenarios on the nonlinear dynamic behaviour of studied RC bridges by employing the IDA approach. To conduct IDAs, a sufficient number of earthquake records should be applied to the structure with an incrementally increased intensity level. The details of the selected ground motion suite are described in the next section.

4.1 Ground Motion Selection

In this study to carry out the IDAs, a set of 32 individual ground motion records is selected from the far-field earthquakes provided in FEMA P695 [49]. Fig. 10 shows the individual and median spectral acceleration response of the selected strong ground motions assuming a 5% damping ratio. In this figure, the fundamental period of the uncorroded bridge (Scenario 1) in transverse vibration is also shown by a vertical dashed line. It is noteworthy that the second vibration mode of the reference bridge specimen is its primary transverse mode. As shown in Fig. 10, the spectral acceleration response of individual records at the fundamental transverse period (Sa (T_2, 5%)) varies from approximately 0.2g to 2.2g, which shows a relatively high scatter. The reason for showing only the fundamental period of the uncorroded bridge in this figure is that the fundamental transverse period of all the studied bridges with different corrosion levels is almost identical. This is because the calculated fundamental period is based on the uncracked stiffness of the components where the contribution of steel reinforcement on lateral stiffness of the structure is negligible.

The intensity level of each selected ground motion record is scaled up from 0 to 2.2g (by 0.1g steps) in terms of Sa(T_2,5%) and used as input for incremental time history analyses. Therefore, 704 nonlinear time history analyses are performed on each bridge specimen listed in Table 2. The results of the IDAs are presented in the next section.

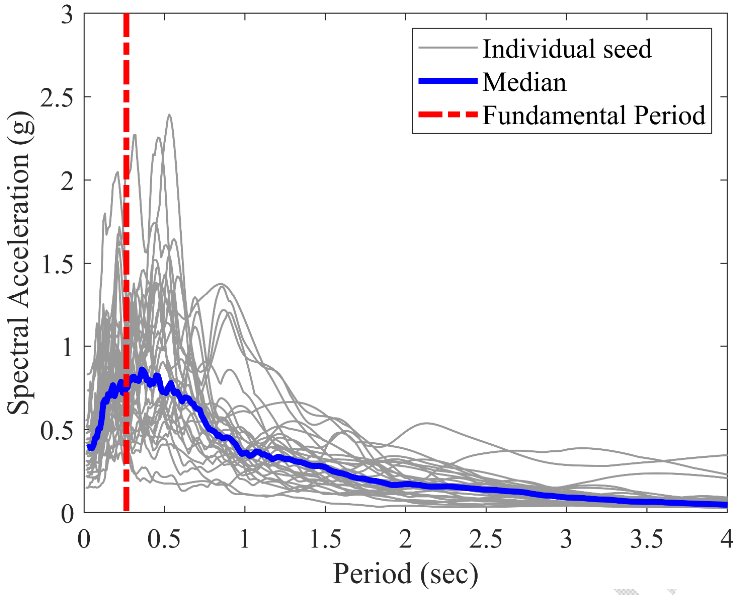

Fig. 10. Spectral acceleration response of selected ground motion suite

4.2 Results and Discussion

Taking the peak drift ratio response of each bent as an engineering demand parameter (EDP), the multi-record and summarised IDA curves are plotted in Figs. (11-12) for Scenario 1 (pristine bridge) and Scenario 3 (extremely symmetrically corroded bridge), respectively.

Fig. 11 shows that median IDA curves of all bents become a plateau at Sa(T_2, 5%)=1.2g. However, a simple comparison between the median IDA curves indicates that a given intensity level of ground motions induces higher drift ratios in bent 1. For instance, while Sa(T_2, 5%)=1g results in approximately 0.038 peak drift ratio in columns of bent 1, the same median intensity level of ground motions causes about 0.019 and 0.022 peak drift ratios in columns of bent 2 and bent 3, respectively. This shows the higher vulnerability of bent 1 in the uncorroded bridge specimen. However, as Fig. 12 shows, the median IDA response of all bents in extremely symmetrically corroded bridge specimen (Scenario 3) is approximately the same, where a slight level of input earthquake records leads to a brittle collapse mode of the bents at less than 0.01 peak drift ratios. The reason can be attributed to the insufficient level of confinement in the piers of this bridge due to the premature fracture of severely corroded spirals.

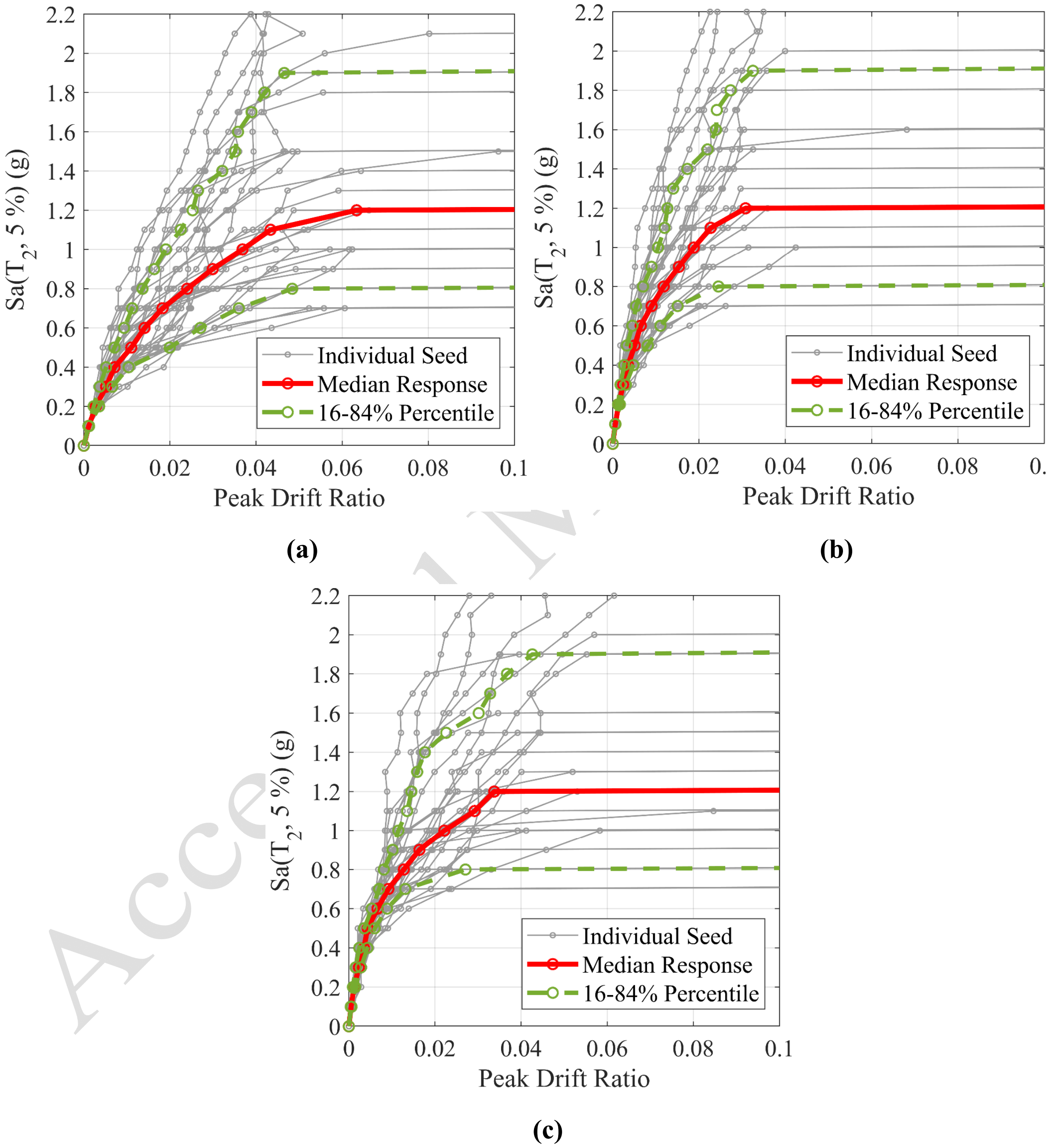

Fig. 11. Multi-record and summarised IDA curves for Scenario 1: (a) bent 1, (b) bent 2, and (c) bent 3.

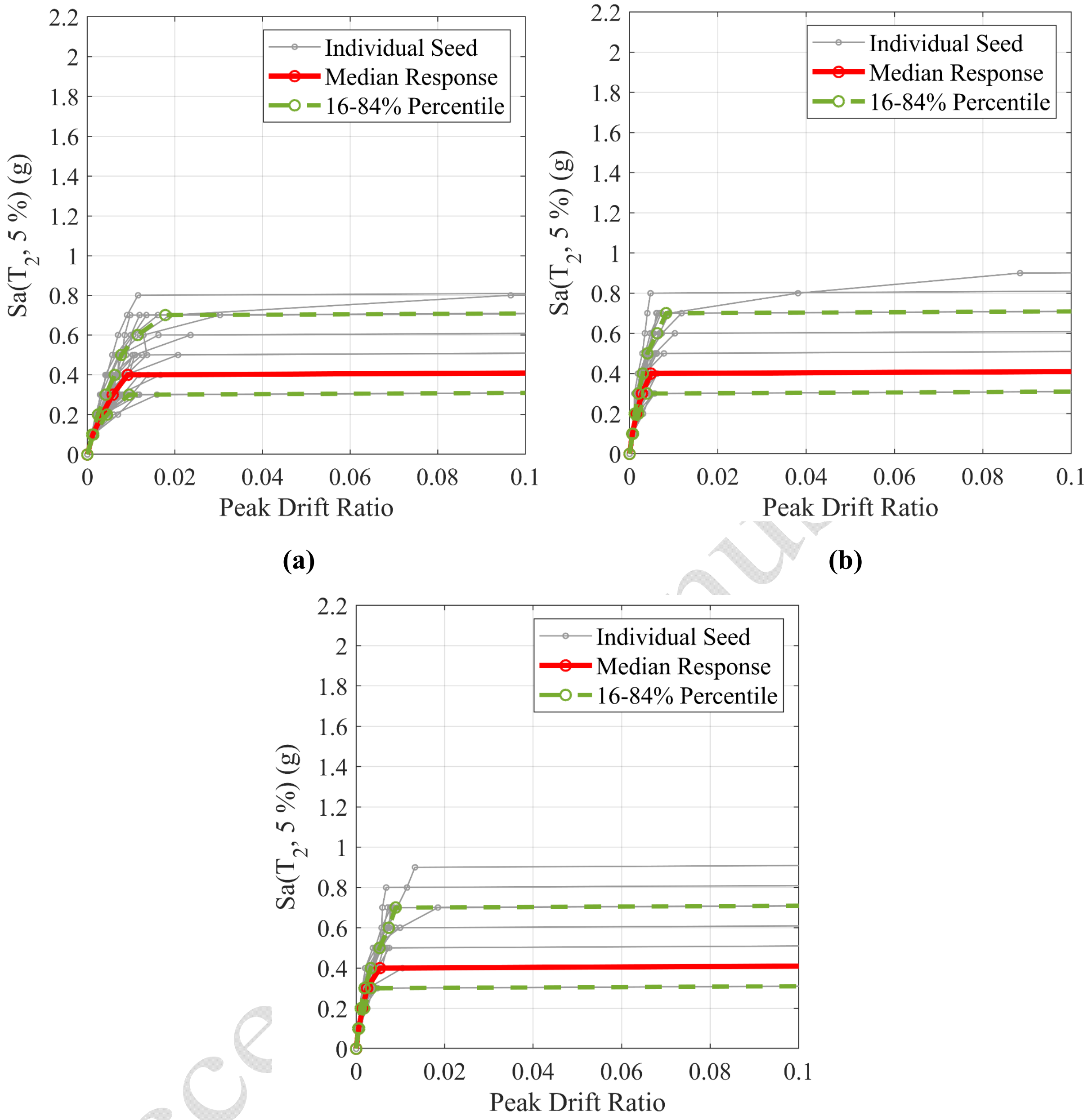

(c)

Fig. 12. Multi-record and summarised IDA curves for Scenario 3: (a) bent 1, (b) bent 2, and (c) bent 3.

In order to investigate the nonlinear behaviour and failure mechanism of the hypothetical bridge configurations, in Fig. 13, the median IDA response of each bent is compared both in the global (Figs. 13(a), 13(c), 13(e), 13(g), 13(i)) and the local scales (Figs. 13(b), 13(d), 13(f), 13(h), 13(j)). Further, the collapse limit state (LS) of each bent, taken from the pushover analysis results (Fig.

9), is shown by a vertical line. The intersection of the collapse LS threshold and the corresponding median IDA curve yields the median intensity level associated with the onset of failure of each bent. Moreover, using the maximum compressive strain demand of core concrete at the critical section of columns, a simple metric for the progression of local damage is considered as follows:

$$\mathrm{CFI} = 1 - \frac{\varepsilon_{c,\max}}{\varepsilon_{uc,u}} \tag{6}$$

where CFI is an abbreviation for Concrete Failure Index and $\varepsilon_{c,max}$ is the maximum compressive strain demand in core concrete at each intensity level. The reason for considering the core concrete failure as the onset of the collapse of piers at the material scale was discussed in Section 3. The lower the CFI value, the higher the extent of damage in core concrete. Therefore, CFI=0 corresponds to the failure (crushing) of core concrete. By calculating the median amount of CFI for each intensity level of applied ground motion records, the median Sa(T_2,5%)) against CFI response of each bent can be plotted. It is worth highlighting that the reason for selecting the response of core concrete as an indicator of damage in the material scale is that, as the results of pushover analysis show (Fig. 9), the failure of all bents with various corrosion levels is governed by the crushing of core concrete. Likewise, the results presented in Fig. 13 confirm this assumption.

Figs. 13(a-b) compares the median IDA response of all bents in Scenario 1. From Fig. 13 (a), it can be inferred that the failure threshold of bent 1 reaches a less earthquake intensity level than the other bents. This can be better explained by the variation of CFI as presented in Fig. 13(b), where the median concrete failure occurs at Sa(T_2, 5%)= 0.8g, whereas it takes place at Sa(T_2, 5%)= 1g and Sa(T_2, 5%)= 1.2g for bents 2 and 3, respectively.

Figs. 13(c-d) show the median IDA response of bents in the slightly symmetrically corroded RC bridge (Scenario 2). Comparing the results presented in these figures with Figs.13(a-b) show that the slight symmetrical corrosion of piers has caused a 25% reduction in the associated intensity level with the plateau response of bents. However, the sequence of failure of bents has not experienced a significant change, where bent 1 sustains higher displacement demands.

Figs.13(e-f) show that the significant reduction in the capacity of bents due to the severe symmetrical corrosion of piers results in near-synchronised flexural failure of all piers. Therefore, it can be inferred from the results given in Figs.13(e-f) that all the bents fail almost simultaneously for the RC bridge supported on severely symmetrically corroded unequal-height piers. However, this conclusion is different from the expected response of uncorroded irregular bridges, where due to the asymmetrical distribution of seismic demands in the piers of varying heights, sequential failure is more expected. The near-simultaneous flexural failure of severely corroded piers can be better understood by comparing the variation of CFI (Fig. 13(f)). Fig. 13(f) shows that the failure of core concrete occurs at approximately the same intensity level in all bents. This can be attributed to the premature fracture of highly corroded transverse reinforcement, where the core concrete behaves almost like unconfined concrete. This causes a brittle failure mode in the severely corroded columns.

Figs. 13(g-h), gives the outputs of IDAs in global and local scales for asymmetrically corroded bridge specimen, Scenario 4. As discussed in section 2.5 and shown in Table 2, the columns of the intermediate bent are severely corroded for this bridge scenario, while the other bridge columns are just slightly affected by corrosion. Fig. 13(g) indicates that the onset of failure of taller columns (columns of bent 2) coincides with that of shorter columns (columns of bent 3). Comparing these results with those of the reference bridge given in Fig. 13(a) implies that the higher ductility demand on the relatively stiffer piers of bent 3 is regulated considerably by the greater corrosion level of bent 2. Consequently, the columns of these two bents with different stiffnesses are collapsed at approximately the same intensity of input ground motions. Moreover, Fig. 13(h) indicates that up to Sa(T_2, 5%)=0.375g, the calculated median value of CFI for bent 2 is lower than others. For instance, for Sa(T_2, 5%)=0.3g, the median value of CFI for bent 2 is approximately 0.72, whereas it is around 0.85 and 0.9 for bents 1 and 3, respectively. However, the CFI of bent 1 becomes the least between all bents for higher intensities. For example, for Sa(T_2, 5%)=0.5g, the value of CFI is calculated as 0.28, 0.56, and 0.75 for bent 1, bent 2 and bent 3, respectively. This is because, for higher input intensity levels, once the severely corroded columns (in bent 2) enter the nonlinear range (due to the rebar yielding) and lose their stiffness, the re-distribution of seismic demands applies higher lateral forces on bent 1. However, this conclusion is drawn based on the median response (Fig. 13(h)), and for individual ground motion with varied frequency content, other reasons might alter the re-distribution of demands (e.g., yielding of bent 3).

Finally, Figs. 13(i-j) present the IDA results of bridge Scenario 5. The stiffer bent (with the shorter piers) is severely corroded in this bridge, whereas the other two bents are slightly corroded. As shown in Figs. 13(i-j), the asymmetrical corrosion scenario has resulted in the near-synchronised collapse of bent 1 and bent 3 at Sa(T_2, 5%)=0.6g.

Moreover, comparing Fig. 13(j) with Fig. 13(b) confirms that, for a given ground motion intensity, the CFI of bent 3 in bridge Scenario 5 becomes remarkably closer to that of bent 1. This implies that the asymmetrical corrosion of piers results in an adjusted extent of damage in piers of this bridge specimen due to the relatively balanced distribution of deformation demands between the piers. Therefore, it can be concluded that the seismic behaviour of an irregular RC bridge located in an aggressive environment notably depends on the corrosion scenario of the piers, where the expected unbalanced seismic demand might be turned into a relatively balanced distribution of demands during the time. Consequently, the damage mechanism and progression of failure in different piers might be changed.

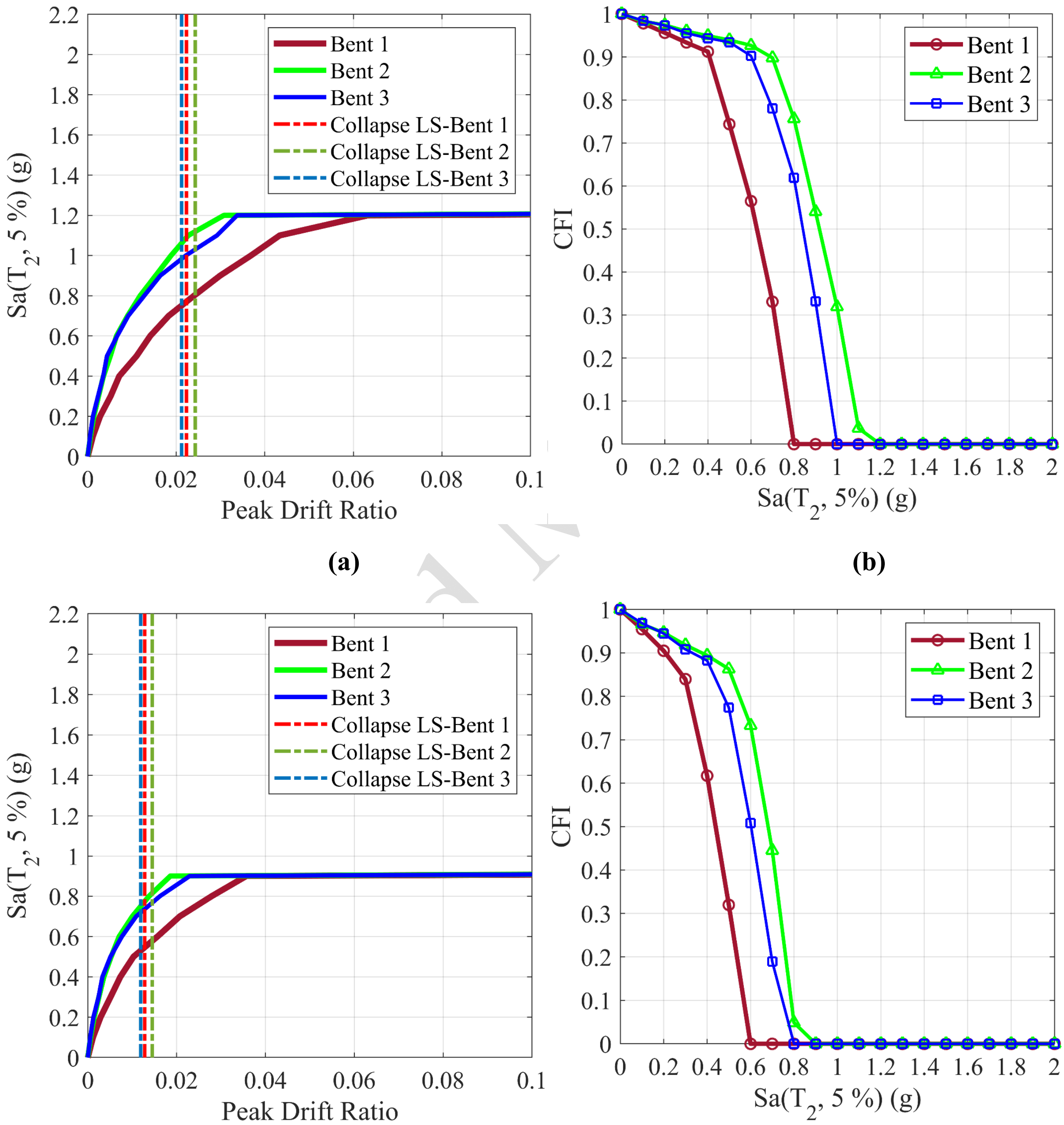

(a) (b)

(c) (d)

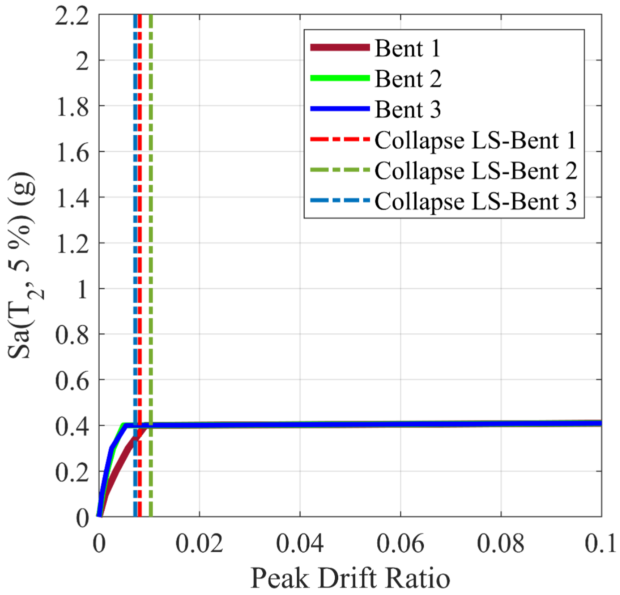
Bent 1
Bent 2
Bent 3
Collapse LS-Bent 1
Collapse LS-Bent 2
Collapse LS-Bent 3
Sa(T2, 5 %) (g)
Peak Drift Ratio

(e)

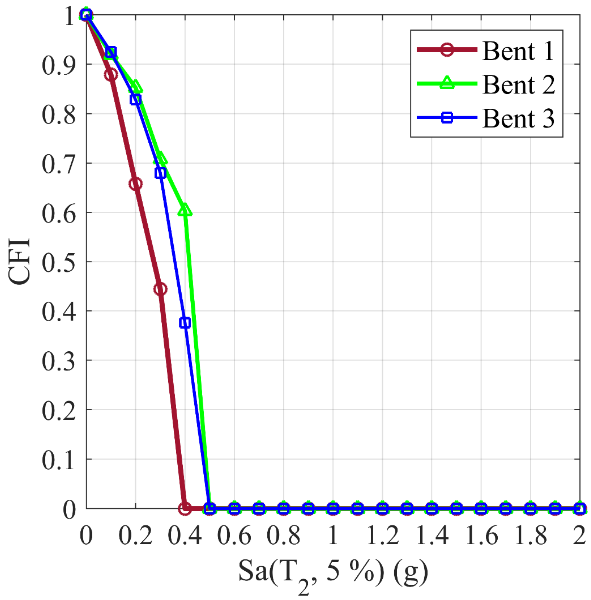
Bent 1
Bent 2
Bent 3
CFI
Sa(T2, 5 %) (g)

(f)

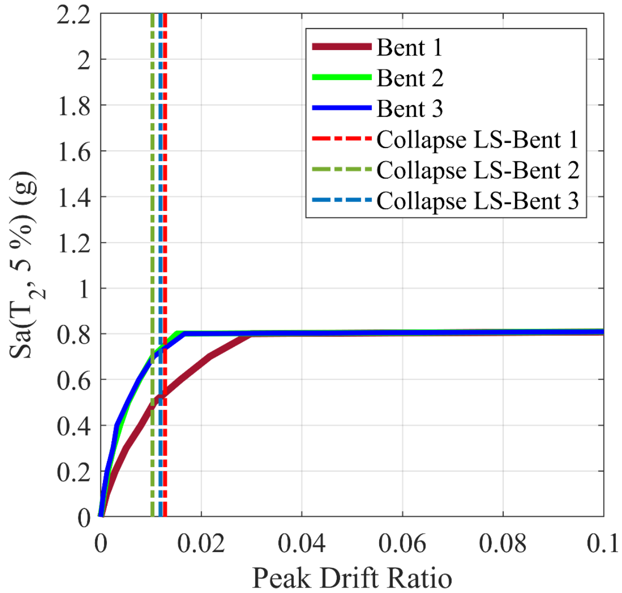
Bent 1
Bent 2
Bent 3
Collapse LS-Bent 1
Collapse LS-Bent 2
Collapse LS-Bent 3
Sa(T2, 5 %) (g)
Peak Drift Ratio

(g)

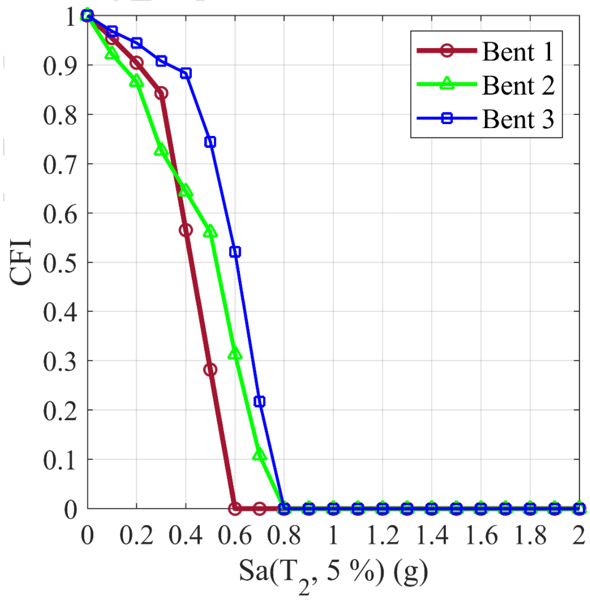
Bent 1
Bent 2
Bent 3
CFI
Sa(T2, 5 %) (g)

(h)

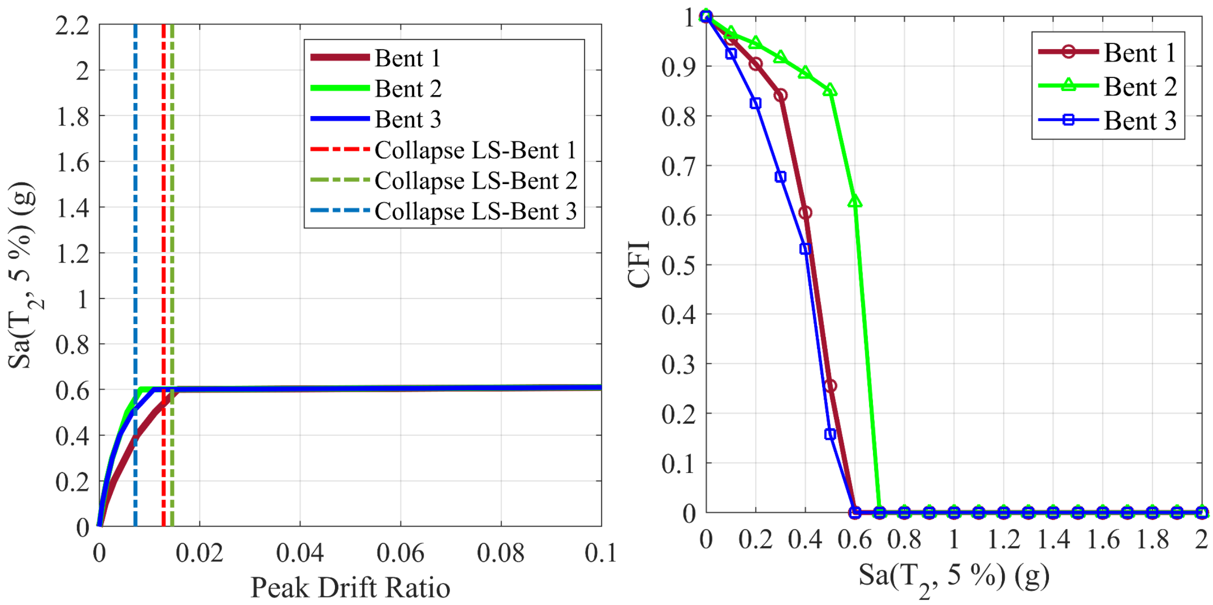

(i) **(j)**

Fig. 13. Median IDA outputs in global and local scales: (a-b) Scenario 1; (c-d) Scenario 2; (e-f) Scenario 3; (g-h) Scenario 4, and (i-j) Scenario 5

5. Time-Dependent Fragility Analysis

This section develops time-dependent fragility curves for the reference bridge with different corrosion scenarios. To this end, the conditional exceedance probability of a particular LS given that Intensity Measure (IM) equals x can be obtained from Eq. (7):

$$P\left(EDP \geq LS \mid IM = x\right) = 1\text{-}\Phi\left(\frac{\ln(\mathrm{LS}) - \ln(\mu)}{\beta}\right) \tag{7}$$

where $P(.)$ is the probability that EDP (here EDP is peak drift ratio) exceeds a specific LS given that the IM (here IM is Sa(T_2, 5%)) of input ground motion equals x. Further, $\Phi(.)$ is the lognormal distribution function, and $\ln(\mu)$ and β are the logarithmic mean and logarithmic standard deviation values of EDP, respectively.

Here, the focus is on comparing the collapse probability of different bents in any considered corrosion scenarios. Therefore, the drift ratio associated with concrete crushing (noted as Δ_c in Table 3) of piers is assumed as the collapse LS in Eq. (7). Then, using the outputs of IDAs, the collapse probability of each bent with different corrosion scenarios are plotted in Fig. 14.

As shown in Fig. 14(a), the collapse probability of bent 1 is higher than other bents for the reference bridge (Scenario 1). For instance, for IM=1g, while the collapse probability of bent 1 is approximately 82%, it is around 50% and 38% for bent 3 and bent 2, respectively. Likewise, in Fig. 14(b), the same trend can be seen with a slightly higher probability of collapse due to the symmetrical corrosion of piers. However, as Fig. 14(c) shows, in bridge case 3, the fragility curves of bent 2 and bent 3 get much closer to that of bent 1. Especially for higher IMs (i.e., higher than IM=0.6g), the probability of collapse of all bents is approximately the same. For example, for IM=0.7g, the collapse probability of bent 1, bent 2 and bent 3 are approximately 99%, 92%, and 95%, respectively. This reminds the near-synchronised brittle failure of bents, which is consistent with the conclusion drawn for the results presented in Figs. 13(e-f).

Fig. 14(d) compares the collapse probability of all bents in the asymmetrically corroded bridge Scenario 4. As can be seen in this figure, due to the higher degree of corrosion in middle columns, the fragility curves of bent 3 and bent 2 supported by the tallest and shortest piers are similar. This implies the synchronised failure of these two bents just after the failure of bent 1.

Finally, Fig. 14(e) displays the fragility curves for bridge Scenario 5, where the shorter columns are extremely corroded whereas the remaining columns are slightly corroded. This figure shows a varied trend, where the fragility curve of bent 3 is on top of others. This shows that the probability of collapse of shorter bent is greater than other bents in this scenario. Therefore, it can be concluded that different corrosion scenarios lead to diverse seismic performance and failure sequences of multi-span RC bridges with substructure irregularity.

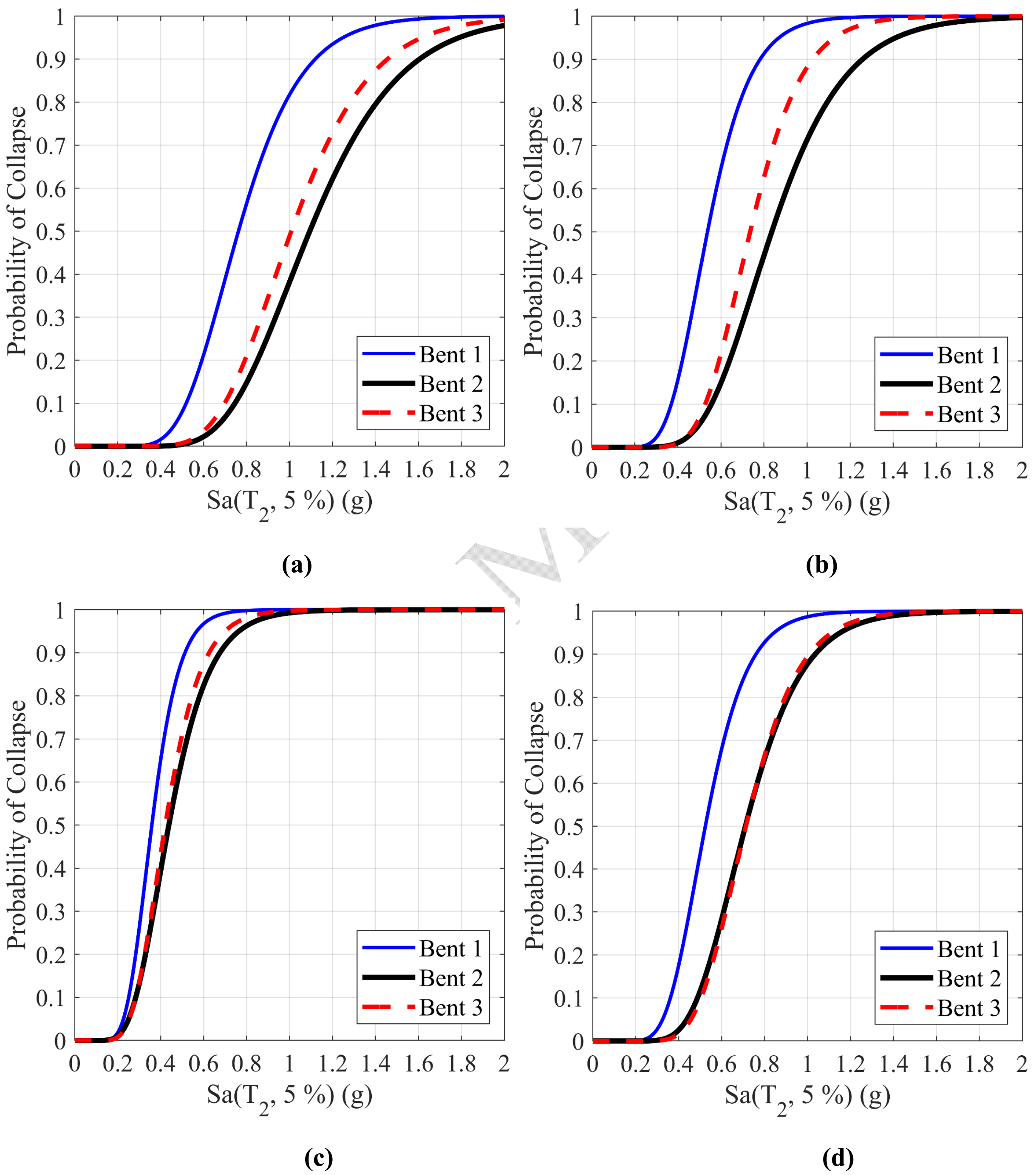

(a) (b) (c) (d)

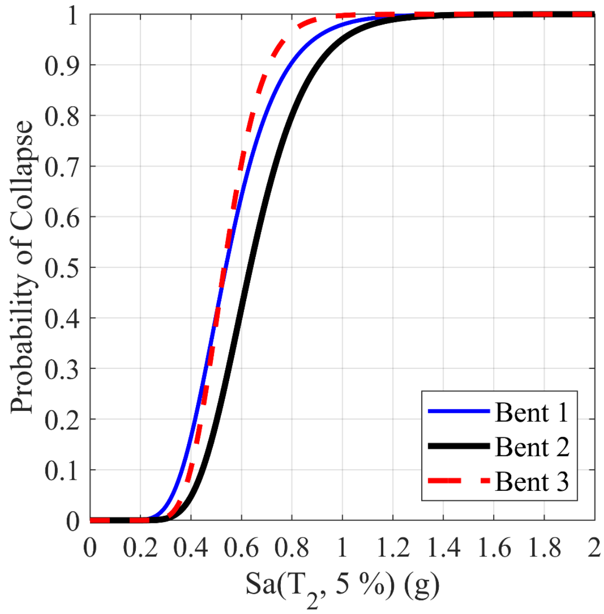

(e)

Fig. 14. Collapse probability of each bent in: (a) Scenario 1; (b) Scenario 2; (c) Scenario 3; (d) Scenario 4, and (d) Scenario 5

6. Conclusions

This paper focused on the seismic performance and vulnerability analysis of multi-span RC bridges with unequal height piers subject to different corrosion scenarios. An advanced three-dimensional nonlinear FE model was developed to simulate the nonlinear dynamic response of multi-span RC bridges. The accuracy of the developed FE model was then successfully verified against the large-scale shake table test results of an irregular two-span RC bridge specimen. A reference two-span RC bridge specimen with unequal height pristine piers, and four hypothetical corroded bridges with different corrosion scenarios, including symmetrical and asymmetrical corrosion scenarios, were studied. Subsequently, failure modes and nonlinear dynamic behaviour of studied bridges with varied corrosion scenarios were analysed using nonlinear pushover and IDAs results. Finally, the corrosion-dependent fragility curves were developed for each hypothetical scenario to quantify the influence of different corrosion scenarios of piers on the vulnerability of the considered bridge layouts. Results show that:

- In the reference bridge (Scenario 1), the unbalanced distribution of seismic ductility demands due to the substructure stiffness irregularity causes the earlier failure of medium-height piers. This triggers the higher vulnerability of bent 1 in this bridge specimen.
- The slight symmetrical corrosion level (around 5.5% in terms of rebar mass loss, t=5 years) of the bridge columns (Scenario 2) causes an approximately 25%, 35%, and 20% reduction in median failure IM of bent 1, bent 2, and bent 3, respectively. However, it does not affect the failure sequence of bents, where bent 1 tolerates higher seismic ductility demands than other bents.
- The severe symmetrical corrosion of bridge piers results in near-synchronised flexural failure of bents of varying heights. This is due to insufficient confinement in severely symmetrically corroded bridge columns resulting in their brittle flexural failure mode. The results of seismic fragility analysis confirm this conclusion, where particularly for higher IM values, the failure probability of all bents is near identical.
- Depending on the hypothetical corrosion scenario, the asymmetrical corrosion of piers in an irregular concrete bridge structure can regulate/exacerbate the unbalanced distribution of seismic ductility demands in piers of varying heights. For instance, results show that the adjusted seismic ductility demand on highly corroded bent 2 (Scenario 4) results in the simultaneous failure of shorter and taller columns.

It is worth mentioning that the results obtained in this study are valid for the selected bridge layout and corrosion scenarios. Therefore, further investigations are needed to evaluate the seismic performance of other ageing RC bridges with varied structural configurations and different corrosion morphologies. Nevertheless, this study lays a scientific foundation for future research in vulnerability assessment of corrosion-damaged irregular multi-span RC bridges subject to seismic hazard.

CRediT author statement

Ebrahim Afsar Dizaj: Writing original draft, Methodology, Conceptualization, Finite Element Modelling, Validation, Formal Analysis. **Mohammad Reza Salami:** Methodology, Investigation, Visualization, Modal Analysis, Review & Editing, Resources. **Mohammad Mehdi Kashani:** Supervision, Review & Editing, Visualization.

Declaration of Competing Interest

The authors declare that they have no known competing financial interests or personal relationships that could have appeared to influence the work reported in this paper.

References

1. AASHTO. (2012). AASHTO LRFD bridge design specifications, Washington, DC.
2. BSI (British Standards Institution). (1998). Eurocode 8: design of structures for earthquake resistance–Part 2: bridges. BS EN 1998-2 (2005), London.
3. Comptroller and Auditor General, Maintaining Strategic Infrastructure: Roads, HC 169, Department for Transport and Highways Agency, London, 6 June 2014.
4. American Society of Civil Engineers. Report card for America's infrastructure. http://www.infrastructurereportcard.org, 2021.

5. Ghosh J and Sood P. Consideration of time-evolving capacity distributions and improved degradation models for seismic fragility assessment of aging highway bridges. Reliability Engineering & System Safety, 2016; 154: 197–218. https://doi.org/10.1016/j.ress.2016.06.001.
6. Domaneschia M, Pellecchia C, De Iuliis E, Cimellaro G.P, Morgese M, Khalil A.A., Ansari F. Collapse analysis of the Polcevera viaduct by the applied element method. Engineering Structures, 2020; 214: 110659. https://doi.org/10.1016/j.engstruct.2020.110659.
7. Broomfield, J.P. Corrosion of Steel in Concrete, Understanding, investigation and repair. Taylor & Francis, London, 2007.
8. Angst U.M. Challenges and opportunities in corrosion of steel in concrete. Materials and Structures, 2008; 51, 4. https://doi.org/10.1617/s11527-017-1131-6.
9. Kawashima K, Aydan O, Aoki T, Kishimoto I, Konagai K, Matsui T, Sakuta J, Takahashi N, Teodori SP, & Yashima A. Reconnaissance Investigation on the Damage of the 2009 L'Aquila, Central Italy Earthquake, Journal of Earthquake Engineering, 2010; 14(6): 817-841. DOI: 10.1080/13632460903584055.
10. Afsar Dizaj E, Kashani MM. Numerical investigation of the influence of cross-sectional shape and corrosion damage on failure mechanisms of RC bridge piers under earthquake loading. Bull Earthquake Eng 2020; 18: 4939–4961. https://doi.org/10.1007/s10518-020-00883-3.
11. Afsar Dizaj E, Kashani MM. Nonlinear Structural Performance and Seismic Fragility of Corroded Reinforced Concrete Structures: Modelling Guidelines. European Journal of Environmental and Civil Engineering, 2021. https://doi.org/10.1080/19648189.2021.1896582.

12. Alipour A, Shafei B, Shinozuka M. Performance evaluation of deteriorating highway bridges located in high seismic areas. Journal of Bridge Engineering, 2011; 6, 597-611. https://doi.org/10.1061/(ASCE)BE.1943-5592.0000197.

13. Biondini F, Camnasio E, & Palermo A. Lifetime seismic performance of concrete bridges exposed to corrosion. Structure and Infrastructure Engineering, 2014; 10(7): 880-900. https://doi.org/10.1080/15732479.2012.761248.

14. Cheng H, Wang DS, Li HN, Zou Y. Investigation on Ultimate Lateral Displacements of Coastal Bridge Piers with Different Corrosion Levels along Height. Journal of Bridge Engineering, 2021. https://doi.org/10.1061/(ASCE)BE.1943-5592.0001696.

15. Choe DE, Gardoni P, Rosowsky D, Haukaas T. Seismic fragility estimates for reinforced concrete bridges subject to corrosion. Structural Safety, 2009; 31(4): 275–83. https://doi.org/10.1016/j.strusafe.2008.10.001.

16. Ghosh J, Padgett JE. Aging considerations in the development of time-dependent seismic fragility curves. J Struct Eng 2010; 136(12):1497–1511. https://doi.org/10.1061/(ASCE)ST.1943-541X.0000260.

17. Ni Choine M, Kashani MM, Lowes LN, O'Connor A, Crewe AJ, Alexander NA. Nonlinear dynamic analysis and seismic fragility assessment of a corrosion damaged integral bridge. International Journal of Structural Integrity, 2016; 7(2): 227–239. https://doi.org/10.1108/IJSI-09-2014-0045.

18. Yuan W, Guo A, Li H. Seismic failure mode of coastal bridge piers considering the effects of corrosion-induced damage. Soil Dynamics and Earthquake Engineering, 2017; 93:135–146. https://doi.org/10.1016/j.soildyn.2016.12.002.

19. Dizaj EA, Madandoust R, Kashani MM. Exploring the impact of chloride-induced corrosion on seismic damage limit states and residual capacity of reinforced concrete structures. Struct Infrastruct Eng 2018; 14(6): 714–729. https://doi.org/10.1080/15732479.2017.1359631.

20. Guirguis JEB, Mehanny SSF. Evaluating code criteria for regular seismic behavior of continuous concrete box girder bridges with unequal height piers. J Bridge Eng 2012; 18(6):486–498. DOI: 10.1061/(ASCE)BE.1943-5592.0000383.

21. Araujo M, Marques M, and Delgado R. Multidirectional pushover analysis for seismic assessment of irregular-in-plan bridges. Engineering Structures, 2014; 79: 375–389. https://doi.org/10.1016/j. engstruct.2014.08.032.

22. Akbari R. Seismic fragility analysis of reinforced concrete continuous span bridges with irregular configuration. Struct Infrastruct Eng 2012; 8: 873–889. https://doi.org/10.1080/15732471003653017.

23. Akbari R, and Maalek S. A review on the seismic behaviour of irregular bridges. Proceedings of the Institution of Civil Engineers-Structures and Buildings, 2018; 171(7): 552-580.

24. Grendene M, Franchetti P, and Modena C. Regularity criteria for RC and PRC multispan continuous bridges. Journal of Bridge Engineering, 2012; 17(4): 671–681. https://doi.org/10.1061/(ASCE)BE.1943-5592.0000267.

25. Jara JM, Reynoso JR, Olmos BA and Jara M. Expected seismic performance of irregular medium-span simply supported bridges on soft and hard soils. Engineering Structures, 2015; 98: 174–185, https://doi.org/10.1016/j.engstruct.2015.04.032.

26. Kappos AJ, Manolis GD, Moschonas IF. Seismic assessment and design of R/C bridges with irregular configuration, including SSI effects. Eng Struct 2002; 24(10): 1337–1348. https://doi.org/10.1016/S0141-0296(02)00068-8.

27. Kohrangi M, Bento R, & Lopes M. Seismic performance of irregular bridges–comparison of different nonlinear static procedures. Structure and Infrastructure Engineering, 2015; 11(12): 1632-1650. https://doi.org/10.1080/15732479.2014.983938.

28. Rezaei H, Arabestani S, Akbari R, and Farsangi EN. The effects of earthquake incidence angle on the seismic fragility of reinforced concrete box-girder bridges of unequal pier heights. Structure and Infrastructure Engineering, 2022; 18(2): 278-293. https://doi.org/10.1080/15732479.2020.1842467.

29. Soleimani F, Vidakovic B, DesRoches R, Padgett J. Identification of the significant uncertain parameters in the seismic response of irregular bridges. J Eng Struct 2017; 141: 356–72. http://dx.doi.org/10.1016/j.engstruct.2017.03.017.

30. Soltanieh S, Memarpour MM, Kilanehei F. Performance assessment of bridge-soil-foundation system with irregular configuration considering ground motion directionality effects. Soil Dyn Earthq Eng 2019; 118: 19–34. https://doi.org/10.1016/j.soildyn.2018.11.006.

31. Xiang N, Li J. Utilizing yielding steel dampers to mitigate transverse seismic irregularity of a multispan continuous bridge with unequal height piers. Engineering Structures, 2020; 110056. https://doi.org/10.1016/j.engstruct.2019.110056.

32. Panchireddi B, & Ghosh J. Cumulative vulnerability assessment of highway bridges considering corrosion deterioration and repeated earthquake events. Bulletin of Earthquake Engineering, 2019; 17(3): 1603–1638. doi:10.1007/s10518-018-0509-3.

33. Zhang Y, DesRoches R, Tien I. Impact of corrosion on risk assessment of shear-critical and short lap-spliced bridges. Engineering Structures, 2019; 189: 260-271. https://doi.org/10.1016/j.engstruct.2019.03.050.

34. Johnson N, Ranf RT, Saiidi MS, Sanders D, and Eberhard M. Seismic testing of a two-span reinforced concrete bridge. Journal of Bridge Engineering, 2008; 13(2): 173-182. https://doi.org/10.1061/(ASCE)1084-0702(2008)13:2(173).

35. McKenna F. OpenSees: A framework for earthquake engineering simulation. Computing in Science & Engineering. 2011; 13(4): 58–66. doi:10.1109/MCSE.2011.66.

36. Kashani MM, Lowes LN, Crewe AJ, and Alexander NA. Nonlinear fibre element modelling of RC bridge piers considering inelastic buckling of reinforcement. Engineering Structures, 2016; 116: 163–177. https://doi.org/10.1016/j.engstruct.2016.02.051.

37. Mander JB, Priestley MJN, Park R. Observed stress–strain behavior of confined concrete. J Struct Eng 1988; 114(8): 1827–1849. https://doi.org/10.1061/(ASCE)0733-9445(1988)114:8(1827).

38. Kashani MM, Lowes LN, Crewe AJ, Alexander NA. Phenomenological hysteretic model for corroded reinforcing bars including inelastic buckling and low-cycle fatigue degradation. Computer and Structures, 2015; 156: 58-71. https://doi.org/10.1016/j.compstruc.2015.04.005.

39. Apostolopoulos CA. Mechanical behavior of corroded reinforcing steel bars S500s tempcore under low cycle fatigue. Construction and Building Materials, 2007; 21(7): 1447-1456. https://doi.org/10.1016/j.conbuildmat.2006.07.008.

40. Coronelli D, and Gambarrova P. Structural assessment of corroded reinforced concrete beams: modelling guidelines. Journal of Structural Engineering, 2004; 130(8): 1214–1224. https://doi.org/10.1061/ (ASCE)0733-9445(2004)130:8(1214).
41. Du YG, Clark LA, and Chan AHC. Residual capacity of corroded reinforcing bars. Magazine of Concrete Research, 2005; 57(3): 135–147. https://doi.org/10.1680/macr.2005.57.3.135.
42. Du YG, Clark LA, and Chan AHC. Effect of corrosion on ductility of reinforcing bars. Magazine of Concrete Research, 2005; 57(7): 407–419. https://doi.org/10.1680/macr.2005.57.7.407.
43. Afsar Dizaj E. Modelling strategy impact on structural assessment of deteriorated concrete bridge columns. In Proceedings of the Institution of Civil Engineers-Bridge Engineering, 2021. https://doi.org/10.1680/jbren.21.00003.
44. Afsar Dizaj, E., Salami, M. R., & Kashani, M. M. Seismic vulnerability assessment of ageing reinforced concrete structures under real mainshock-aftershock ground motions. Structure and Infrastructure Engineering, 2021. https://doi.org/10.1080/15732479.2021.1919148.
45. FEMA. HAZUS. Earthquake model, technical manual.Washington DC: Federal Emergency Management Agency, 2003.
46. Ramanathan K, Padgett JE, & DesRoches R. Temporal evolution of seismic fragility curves for concrete box-girder bridges in California. Engineering Structures, 2015; 97:29-46. https://doi.org/10.1016/j.engstruct.2015.03.069.
47. Hwang H, Liu JB, Chiu Y-H. Seismic fragility analysis of highway bridges. http://hdl.handle.net/2142/9267⟩; 2001 [05.03.10].

48. Afsar Dizaj E, Kashani MM. Influence of ground motion type on nonlinear seismic behaviour and fragility of corrosion-damaged reinforced concrete bridge piers. Bulletin of Earthquake Engineering, 2022; 20: 1489–1518. https://doi.org/10.1007/s10518-021-01297-5.
49. FEMA P695. Quantification of building seismic performance factors. Federal Emergency Management Agency, Washington, DC, 2009.